J Paleolimnol (2012) 48:159–173
DOI 10.1007/s10933-012-9611-8

ORIGINAL PAPER

1750 years of large rainfall events inferred from particle size at East Lake, Cape Bounty, Melville Island, Canada

François Lapointe · Pierre Francus · Scott F. Lamoureux · Meriem Saïd · Stéphanie Cuven

Published online: 5 May 2012

Abstract Annual grain-size variation was measured on the varved (annually laminated) lacustrine sediment from Cape Bounty East Lake using an innovative image analysis system. About 7100 images were acquired using a scanning electron microscope and processed to obtain measurement of particles from 2845 varves. Several particle-size distributions indices were calculated and can be linked to high-energy sedimentary facies. Moreover, the coarse grain size (98th percentile) of these high-energy facies is strongly correlated with summer rainfall (and also summer temperature) of instrumental data from nearby stations. Particle-size distributions show a similar trend through time, especially for the standard deviation and the 98th percentile. Climatic reconstruction suggests that Cape Bounty recently experienced an unprecedented increase of rainfall events since ~AD 1920. On the other hand, changes in varve thickness are weakly correlated with the particle-size distribution. Altogether, these results highlight the need to obtain annual grain-size data to identify a meteorological signal.

Keywords Varves · Scanning electron microscope · Image analysis · Grain size · Paleoclimate · High-Arctic

This is one of 18 papers published in a special issue edited by Darrell Kaufman, and dedicated to reconstructing Holocene climate and environmental change from Arctic lake sediments.

Electronic supplementary material The online version of this article (doi:10.1007/s10933-012-9611-8) contains supplementary material, which is available to authorized users.

F. Lapointe (✉) · P. Francus
Institut National de la Recherche Scientifique, Centre Eau Terre et Environnement, Québec, QC G1K 9A9 QC, Canada
e-mail: francois.lapointe@ete.inrs.ca

F. Lapointe · P. Francus
GEOTOP, Geochemistry and Geodynamics Research Center, Montreal, QC H3C 3P8, Canada

S. F. Lamoureux
Department of Geography, Queen's University, Kingston, ON K7L 3N6, Canada

M. Saïd
Département de Mathématiques et Statistique, Université Laval, Avenue de la Médecine, Québec, QC G1V 0A6, Canada

S. Cuven
GEOLAB, Centre National de la Recherche Scientifique, 63057 Clermont Ferrand Cedex 1, France

Introduction

Major changes occurred in Arctic climate during the twentieth century, including an important increase of surface air temperature, particularly between 1970 and 2000 (Moritz et al. 2002). Changes in environmental variables such as precipitation, sea-ice extent, snow

cover, and permafrost have had important impacts on local communities and ecosystems. To better understand these changes beyond the available short instrumental record, long-term proxy climate records are needed from across a wide geographical area. In the western Canadian High Arctic, annually laminated sediments from lakes are the only available records with precise chronological control in an area that lacks tree-ring and ice-core records. Varve thicknesses have been mainly used to reconstruct past summer temperatures in Arctic regional syntheses such as those by Overpeck et al. (1997) and more recently by Kaufman et al. (2009). However, recent studies showed that climate signal recorded by clastic varved sediments may be less straightforward than initially thought (e.g. Cockburn and Lamoureux 2008a; Francus et al. 2008). These studies indicate that caution is needed when calibrating varve thickness (VT) using instrumental data, since sediment accumulation can result from different hydroclimatic and geomorphic processes, such as snowmelt, rain events, and landslides. In addition to VT, grain size measured at the annual scale is a sedimentary parameter with potential to reconstruct paleo-hydroclimatic conditions (Francus et al. 2002; Kaufman et al. 2011). In this paper, we use the methods pioneered by Francus (1998) together with a new image acquisition and analysis software developed at INRS, to obtain grain-size measurements within each varve in a long Arctic lake sequence in order to demonstrate its potential for paleoenvironmental reconstructions and to produce a new long paleoclimate reconstruction with annual resolution.

Study site

Cape Bounty East Lake (hereafter, "East Lake") (74°55′N; 109°33′W; 5 m a.s.l.) is located on the south–central coast of Melville Island, Nunavut, in the western Canadian Arctic Archipelago (Fig. 1). As part of a long-term research program (the Cape Bounty Arctic Watershed Observatory), hydrological, limnological, and sedimentary processes have been investigated and monitored in two adjacent lakes and watershed systems since 2003 (Lamoureux et al. 2006; Cockburn and Lamoureux 2008a, b; Dugan et al. 2009; McDonald and Lamoureux 2009; Laurin 2010; Pautler et al. 2010; Lewis et al. 2011; Stewart and Lamoureux 2011). The East and West lakes (unofficial names) have similar morphologies: both are $\sim$1.5 km^2, and maximum depths are 30 and 34 m, respectively. These monomictic lakes have near-isothermal water columns during most of the year. Each winter, a 1.7- to 2.5-m-thick ice forms, and usually persists as a pan until mid-July or early August. The watershed area of East Lake is 11.6 km^2 and mainly composed of weathered Paleozoic sandstone and shale overlain by late glacial and Holocene regressive marine sediments (Hodgson et al. 1984). The glacioisostatic rebound in the area began after deglaciation $\sim$10 ka ^{14}C BP and became negligible since $\sim$2 ka ^{14}C BP (Hodgson 1989). Temperatures at Cape Bounty are typically above freezing during June–August when snowmelt and occasional rainfall contribute to streamflow. The mean annual temperature is -17.9 °C and total precipitation is

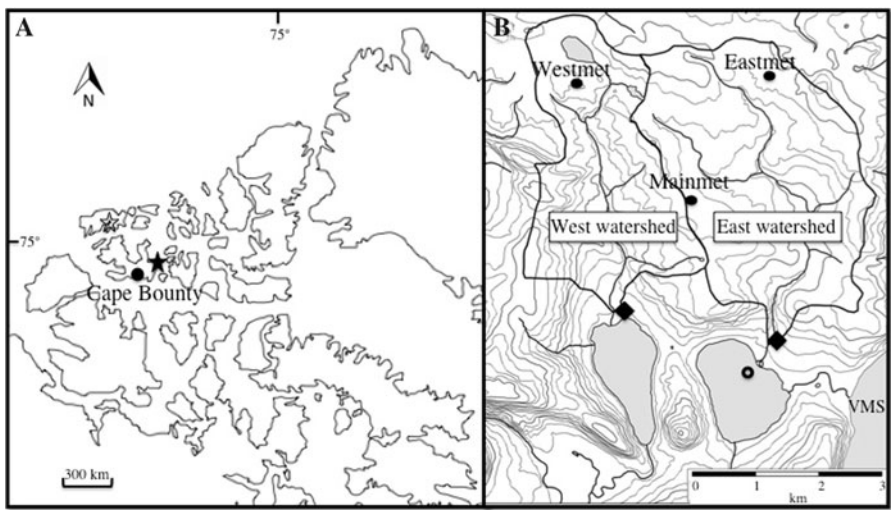

Fig. 1 **A** Location of Cape Bounty (*black circle*) and the weather stations (*black star* = Rea Point; *white star* = Mould Bay). **B** East Lake and West Lake showing their watersheds, weather stations (*black circles*), river gaging stations (*black diamonds*), and core site (*open circle*). *VMS* Viscount Melville Sound

<60 mm/year at Rea Point, the nearest weather station located 105 km to the northeast (Hodgson et al. 1984).

Previous studies

Evolution of the watershed

Cuven et al. (2011) described four principal sedimentary units from a 737-cm-long sediment core from East Lake and developed a 4,200-year-long varve thickness record. Basal unit 1 (which extends from an unknown age to 2192 BC) is massive, and corresponds to the marine stage of the isostatic depression. Unit 2 (2192 BC–AD 243) is finely laminated and interpreted as the transitional period from marine to freshwater conditions. Cuven et al.'s μ-XRF data suggest a decrease of marine influence concomitant with an increase in terrestrial runoff between 400 BC and AD 244. Once East Lake was fully isolated by glacioisostatic uplift from the ocean after AD 244, the sedimentation rate likely increased due to sediment focusing into the smaller lake basin and because of the increased erosion of the exposed unconsolidated marine sediments in the watershed (Cuven et al. 2011). Hence, after AD 244 conditions were more favorable for the formation and preservation of clearly defined clastic varves. In unit 3 (AD 244–1132), varves become clearly defined while the Fe/Mn ratio reaches maximum values, indicating more persistent water column anoxia (Cuven et al. 2011). Unit 4 (AD 1135 to present) has better preserved and thicker laminae.

Sedimentary facies at East Lake

The mechanisms of varve formation at both lakes were inferred from the observation of thin-sections and the monitoring of tributaries and lake water column (Cuven et al. 2010; Cockburn and Lamoureux 2008a, b). Lithozone A is the most common lithofacies and is composed of a fine silt layer deposited by nival melt runoff that is overlaid by a clay cap representing the settling of particles under the ice during winter (Fig. 2). Lithozone B is graded and likely deposited by a turbidity current caused by runoff of higher intensity than the regular spring melt (Fig. 2). Lithozone C is composed of poorly sorted sand layers occurring systematically above the initial snowmelt silt layer and below the clay cap (Fig. 2). It is interpreted to be produced by high-discharge events, which are triggered by high-intensity rainfalls during summer after the snowmelt (Cuven et al. 2010).

Materials and methods

Sediment cores and thin-sections

In June 2006, two cores were retrieved from ice at the deepest (30 m) known location in East Lake (74°53′30.3°N; 109°32′85.5°W): a short gravity corer (CB06G1, 41.5 cm) and a long vibra-corer (CBEV1, 737 cm). These cores were also studied by Cuven et al. (2011). An additional gravity core (07EL01, 42 cm) was retrieved in 2007 from the same location. We used the same thin-sections as those analyzed by Cuven et al. (2011), as well as new sections prepared from core 07EL01 using similar protocols.

Image and grain-size analysis

Thin-section images were acquired using a transparency flatbed scanner at 2400 dpi resolution (1 pixel = 10.6 μm) in plain and cross-polarized light (De Keyser 1999). Using the image analysis software developed at INRS-ETE (Francus and Nobert 2007) and used by Cuven et al. (2011), regions of interest (ROIs) were identified on the flatbed scan digital images. The software then automatically acquired SEM images of the ROIs using a Zeiss Evo® 50 scanning electron microscope (SEM) in backscattered electron (BSE) mode. Eight-bit gray-scale BSE images with a resolution of 1024 × 768 pixels were acquired with an accelerating voltage of 20 kV, a tilt angle of 0° and a 9 mm working distance with a pixel size of 1 μm. These settings optimize contrast between clastic grains and clay matrix (Francus 1998; Soreghan and Francus 2004). Grains within the sedimentary facies appeared black following the transformation of the BSE images into black and white (Francus 1998; Nederbragt and Thurow 2004). Each sedimentary particle was measured for the position of the centre of gravity, area, length of the long and short axis of the best fitting ellipse, and angle of the long axis relative to horizontal (Annex 1 in Supplementary Material) (Francus and Karabanov 2000). Details of the algorithms used here are available in Annex 1 in Supplementary Material. Finally, the size of each particle was calculated according to Francus

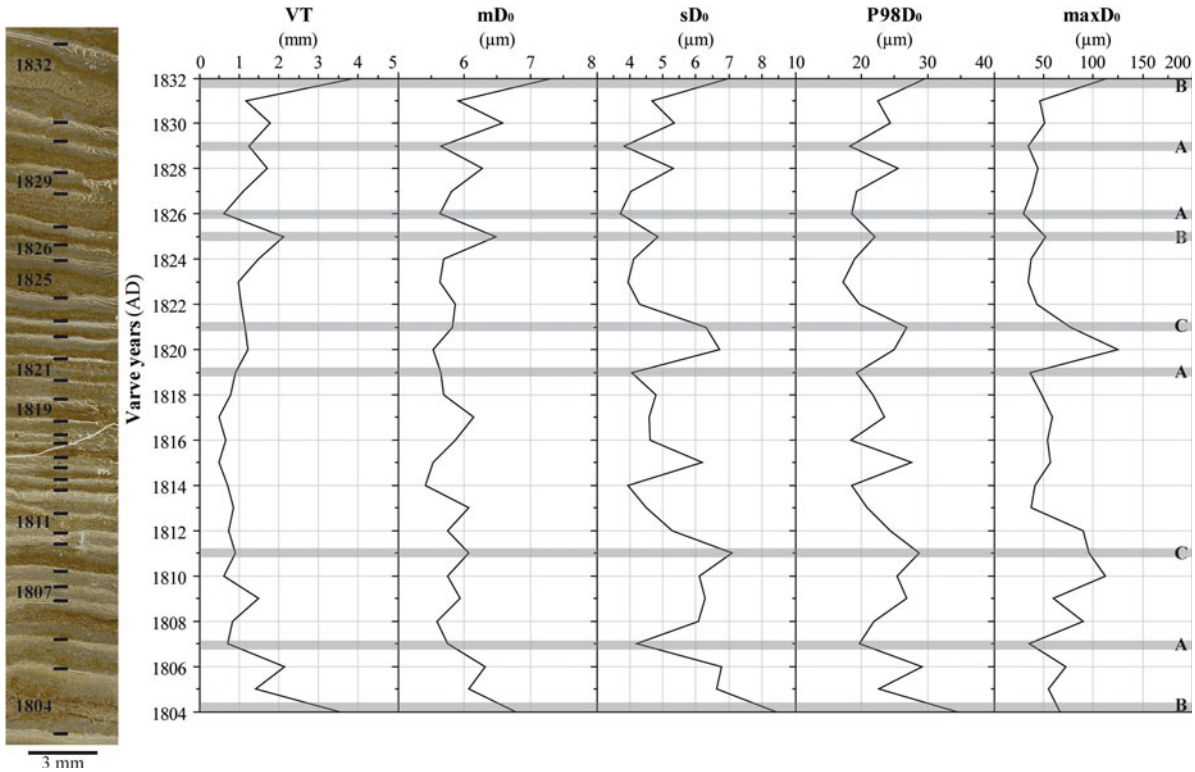

Fig. 2 Thin-section image (*left*) from a flat-bed scanner (*plain-light*) of East Lake sediment showing varve boundaries (*black horizontal bars*) and years. PSD indices (*right*) for AD 1832–1804. *Shaded areas* correspond to the lithozones referred in the text: *A* classic nival deposit, *B* turbidites, *C* debris flow

et al. (2002) in order to determine the following particle-size distribution (PSD) indices for each varve: mD_0 or the median disk apparent diameter (Francus 1998), standard deviation (sD_0), percentile 98 % ($P98D_0$), and maximum ($maxD_0$) (Fig. 2).

PSD indices were analyzed for the last 2845 years (or the upper 359.8 cm) from 6,148 BSE images. When varves were thicker than the size of the image or when the number of grains identified within a single processed image was <900, results from several images were merged in order to obtain representative and robust measurements for each year of sedimentation (Francus and Pirard 2004). Overall, an average of 2.2 images and 1,164 particles were measured for each varve. For technical reasons, grain-size data were only extracted from vibra-core CB06EV1 for which the uppermost sedimentary layer is dated to AD 2000 by cross-dating with surface cores. Usable BSE images could not be acquired from cores 07EL01 and CB06EG1 because of poor sediment impregnation that resulted in incorporation of sanding grit in the sedimentary facies.

Chronology

Radionuclides (^{210}Pb, ^{137}Cs) were measured on core CB06G1 by Cuven et al. (2011). A new varve count was performed using the same set of thin-sections as used by Cuven et al. (2011), except that we included the new 07EL01 surface core. For this new count, we analyzed BSE images in addition to the flatbed scan images (plain and cross-polarized light) of the thin-sections to manually record varve boundaries in the INRS-custom-software. Furthermore, additional BSE images (3072 × 2304 pixels wide and with a pixel size of 3.8 μm) in the uppermost 6 cm of both CB06G1 and 07EL01 cores were assembled in photo-mosaics to observe the lateral variation of sedimentary properties, and hence, to clearly identify each varve. The long core CB06EV1 was cross-

correlated with the short surface core using distinctive marker beds (Lamoureux 2002).

Weather stations

Two meteorological stations were considered for comparison of climate parameters with sediment properties: Rea Point (Station ID: 2403450) and Mould Bay (Station ID: 2502700) located 100 km northeast and 320 km northwest of Cape Bounty, respectively. Temperature, rainfall, and snowfall were extracted from the adjusted historical Canadian climate data (AHCCD) (http://www.cccma.ec.gc.ca/hccd/). Additionally, cumulative melting degree-days (MDD) were calculated using the National Climatological Archive of Meteorological Service Canada.

Statistical methods

For the correlation analyses presented below, we used the Pearson coefficient, denoted r in the sequel. This coefficient is a measure of linear dependence and needs normality for inference purposes. However, extreme values resulting in heavily skewed underlying distributions prevent reliable results. For these reasons, we consider also two non-parametric (rank-based) coefficients, namely Spearman's ρ and Kendall's τ. Spearman's ρ measures the strength of linear dependence between ranks of observations, whereas Kendall's τ is based on concordant/discordant pairs and does not need any hypothesis on linear association (Abdi 2007).

Results[1]

Chronology and error estimation

The uppermost surface of core 07EV1 allowed us to distinguish two additional varves between AD 2000 and 1998. These new varves require that the erosive turbidite recognized by Cuven et al. (2011) be shifted to AD 1971, and reduce the number of eroded years to five, but the rest of our rationale for the upper part of the chronology remains identical to Cuven et al. (2011).

Within the interval where image analysis was performed, we counted 2845 varves over the upper 359.8 cm, or 72 additional couplets compared to Cuven et al. (2011). However differences are larger in some intervals: between 166.7 and 155.5 cm (15.8 %), between 259 and 246.7 cm depth (16.7 %) where varves are more diffuse (Cuven et al. 2011), and between 352.5 and 341.9 cm depth (14.5 %) where varves become very thin (average is 0.47 mm). This new chronology is referred hereafter as the CBEL12a chronology. Figure 3 shows the consistency between the two varve counts made by François Lapointe and Stéphanie Cuven.

Grain-size variations

Sedimentary facies identified by Cuven et al. (2010) can be recognized by PSD indices measured by analysis of BSE images (Fig. 2). Lithozone A, the classic simple nival melt deposit, occurs in AD 1807, 1819, 1826, and 1829, among others, and is characterized by low VT and relatively low values of all PSD indices (Fig. 2A). Lithozone B, caused by runoff of higher intensity than the regular spring melt, formed in AD 1804, 1825, and 1832 and is characterized by high VT and high PSD indices (Fig. 2B). Lithozone C, debris flows likely generated by high rainfall events, such as the one of AD 1811 and 1821 (Fig. 2C), is

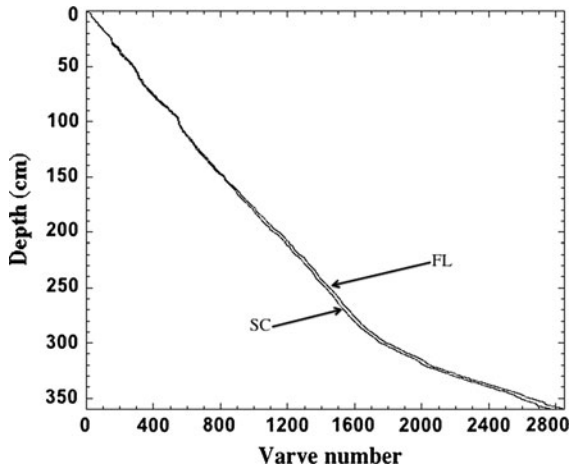

Fig. 3 Comparison between the varve counts from Cape Bounty East Lake by Cuven et al. (2011) (SC) and this study (FL). Varve number 0 was formed in 2000

[1] All of the data from East Lake presented in this study are available on-line through the World Data Center for Paleoclimatology http://www.ncdc.noaa.gov/paleo/pubs/jopl2012arctic/jopl2012arctic.html.

characterized by relatively low VT, average mD_0 but high $P98D_0$, and sD_0 values with coarsest grain size of $\sim$75 μm. Layers with high $P98D_0$ and sD_0 values are poorly sorted and coarse skewed according to the Folk and Ward (1957) graphical method.

The different PSD indices show a number of common and specific trends along the laminated record (Fig. 4). First, mD_0 is relatively low in the lower part of the core but has a clear step increase at $\sim$AD 1350, and shows maximum (coarsest) values in the twentieth century. Both $P98D_0$ and sD_0 exhibit similar variations through time, including the sharp increase at the beginning of the twentieth century, with maximum values in the 1990s. These two indices are strongly correlated ($r = 0.83$, $\rho = 0.84$, $\tau = 0.71$, $p < 0.0001$ for all coefficients). Finally, $maxD_0$ displays a steady, long-term increase toward the top of the core.

Varve thickness and PSD indices

In addition to the test (r, ρ, and τ correlations) on the original time series, we also performed the analysis on the decorrelated versions (Shumway and Stoffer 2000) because the VT series (Fig. 4) exhibit autocorrelations significant up to fourth order, and the PSD series show serial correlation with higher order. Results (Table 1) indicate that almost all correlations are weak but significant, except for Pearson's correlation between VT and $maxD_0$. Removing temporal autocorrelation has a little impact on these results. The strongest, but still relatively weak, correlation between VT and PSD indices is with mD_0. Despite the above-mentioned relatively weak correlation, VT time series (Fig. 4) seems not to be in phase with any of the PSD indices, especially at the beginning of the twentieth century, when VT remains stable, whereas $P98D_0$, sD_0, and

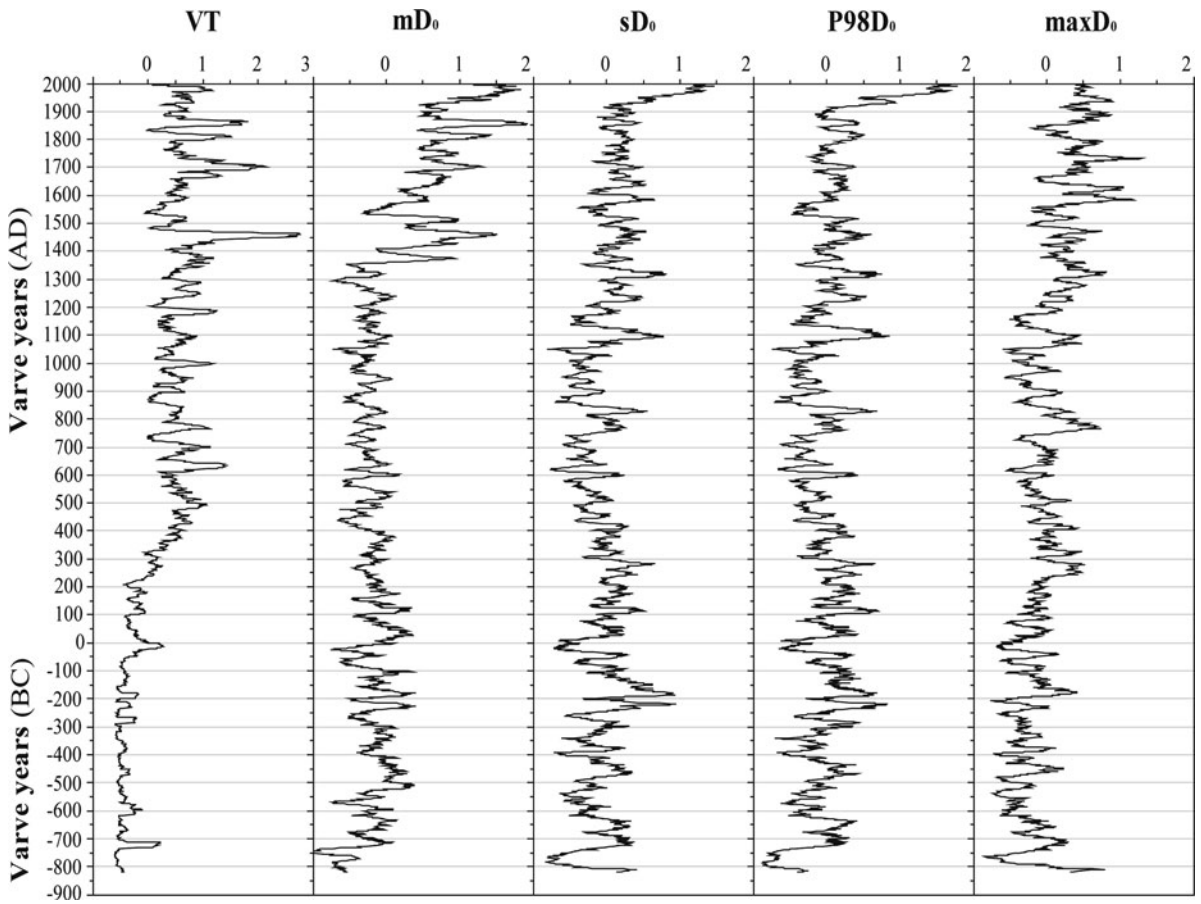

Fig. 4 East Lake varve thickness (VT) and four PSDs indices for the past 2845 years (see text for explanation of indices). Data are standardized relative to the mean and the standard deviation. A 15-year running mean is applied on the series

Table 1 Pearson's (r), Spearman's (ρ), and Kendall's (τ) correlations between varve thickness and annually resolved PSD indices[a], for AD 250–2000, for the raw (top half) and decorrelated (bottom half) time series, and their significance (p values)

Methods	mD_0	sD_0	$P98D_0$	$MaxD_0$
Original time series				
r	0.5343	0.2153	0.2999	0.0426
	(<0.0001)	(<0.0001)	(<0.0001)	(0.0753)
ρ	0.3228	0.1790	0.2618	0.1186
	(<0.0001)	(<0.0001)	(<0.0001)	(<0.0001)
τ	0.2238	0.1217	0.1784	0.0792
	(<0.0001)	(<0.0001)	(<0.0001)	(<0.0001)
Decorrelated time series				
r	0.5503	0.2092	0.3149	0.0166
	(<0.0001)	(<0.0001)	(<0.0001)	(0.4879)
ρ	0.3967	0.1765	0.2745	0.0724
	(<0.0001)	(<0.0001)	(<0.0001)	(0.0025)
τ	0.2745	0.1194	0.1868	0.0483
	(<0.0001)	(<0.0001)	(<0.0001)	(0.0025)

[a] The particle size indices are the median disk apparent diameter: mD_0; the standard deviation: sD_0; the 98th percentile: $P98D_0$; and the maximum: $maxD_0$

mD_0 reach their highest values. For the period spanning ~AD 250–500, VT increases substantially while sD_0 values decrease (Fig. 4). This could be explained by the progressive stabilization of the sedimentary environment as outlined by Cuven et al. (2011).

Calibration with the instrumental record

Data available for correlation are limited: only varves formed after 1971 (above the erosive turbidite) were considered to ensure chronological control. In addition, Mould Bay and Rea Point weather stations changed measurement protocols or stopped operating after 1996 and 1985, respectively. Table 2 summarizes correlations between instrumental meteorological data and PSD index $P98D_0$. The correlations are evaluated from the raw time series because no serial correlation was detected. The strongest positive correlation ($r = 0.85, n = 15, p < 0.001$) is between the largest annual rainfall events at Rea Point and $P98D_0$. Non-parametric correlation coefficients also indicate strong and significant correlations (Table 2).

The linear-regression plot suggests that some extreme values may influence this relationship (Fig. 5). We used the Cook's distances method (Cook and Weisberg 1982) to address this possibility. This is calculated with the following equation:

$$D_t = \frac{1}{\mathrm{MSE}} \sum_{i=1}^{T} \left(\hat{y}_i - \hat{y}_{i(t)}\right)^2 \quad (1)$$

where MSE is the mean squared error, $\hat{y}_i$ is the estimated value of the dependent variable y_i for year i, and $\hat{y}_{i(t)}$ is the fitted value when removing observation t. A value is considered to be influential if $D_t > 1$. As such, no data point is considered influential for the calibration record (Fig. 5B). For linear regression, a

Table 2 Pearson's (r), Spearman's (ρ), and Kendall's (τ) correlations between PSD index $P98D_0$ and instrumental data from Rea Point and Mould Bay and their significance (p values)

Variables	Rea point (1985–1971)			Mould Bay (1996–1971)		
	r	ρ	τ	r	ρ	τ
June temperature (°C)	0.3961	0.3214	0.2000	**0.4907**	**0.5165**	**0.3608**
	(0.1439)	(0.2424)	(0.3282)	(**0.0109**)	(**0.0069**)	(**0.0111**)
July temperature (°C)	0.3788	0.3679	0.2762	0.2459	0.2113	0.1373
	(0.1638)	(0.1779)	(0.1686)	(0.2260)	(0.3000)	(0.3420)
MDD (May–July)	**0.5087**	**0.5893**	**0.4286**	**0.4536**	**0.3737**	**0.2492**
	(**0.0528**)	(**0.0232**)	(**0.0275**)	(**0.0199**)	(**0.0609**)	(**0.0777**)
Largest rainfall (mm)	**0.8479**	**0.7668**	**0.5742**	0.1046	−0.0041	0.0123
	(**0.0001**)	(**0.0009**)	(**0.0035**)	(0.6110)	(0.9841)	(0.9473)
Annual snowfall (cm)	−0.1386	−0.2214	−0.1238	0.0337	0.1246	0.0867
	(0.2471)	(0.4266)	(0.5590)	(0.8729)	(0.5513)	(0.5631)

MDD melting degree-days (°C). Particle size distribution index $P98D_0$ is the 98th percentile. In boldface are values with significant correlations

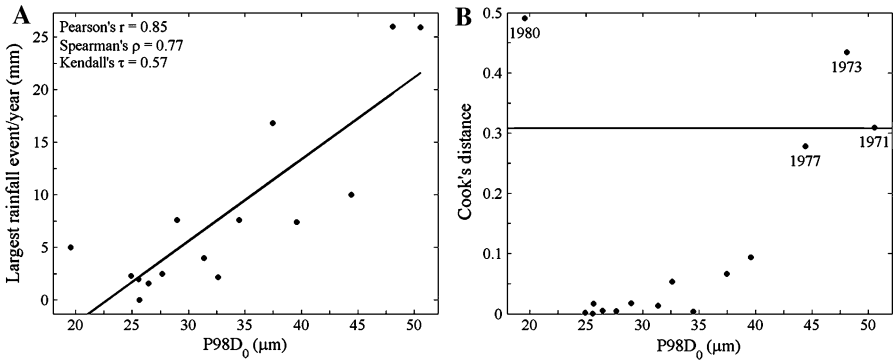

Fig. 5 **A** Linear regressions between $P98D_0$ and largest rainfall event/year at Rea Point (1985–1971), with Pearson's, Spearman's and Kendall's correlations. **B** Cook's distances for linear regression between $P98D_0$ and largest rainfall event/year at Rea Point (1985–1971). *Horizontal line* shows the critical value of $4/(T - 2)$

threshold value $4/(T - 2)$ is used, and D_t values $> 4/(T - 2)$ are usually considered outliers (Cook and Weisberg 1982; Sheather 2009). In our data series, two outliers are above this threshold (Fig. 5B; 0.31). One way to address this problem is to remove the outliers; however, this approach is not attractive because of the small sample size. In addition, removing data points one by one yields 15 regression lines with slopes ranging from 0.669 to 0.889, compared to the slope for all data, which is 0.777. For the maximal $P98D_0$ observation (50.55 μm), these regressions give estimated rainfall from 19.13 to 23.5 mm. Finally, when years 1971, 1973, and 1980 are removed, the resulting regressions lead again to outliers in terms of Cook's distance. When data are contaminated with outliers, another methodology is to use robust rather than ordinary least squares estimation (Rousseeuw and Leroy 1987); however, these two approaches yield approximately equal results when applied to our dataset.

These findings motivated the use of a nonlinear model coupled with robust estimation: the Box–Cox method that yields a log–log transformation (Box and Cox 1964). Because no precipitation (zero value) was recorded in 1979, we added a constant (1 mm) to all rainfall observations to avoid negative log-value. The model then reduces to a linear model in log-transformed variables. For robust estimation, we use the bisquare weighting function (Maronna et al. 2006) (Fig. 6), where

$$\log(\text{rainfall} + 1) = -9.5337 + 3.2706 \log P98D_0. \quad (2)$$

Two other strong correlations between $P98D_0$ and the instrumental record include those with (1) MDD at Rea Point ($\rho = 0.59$, $p = 0.02$), and (2) June temperatures at Mould Bay ($\rho = 0.52$, $p = 0.007$) (Table 2).

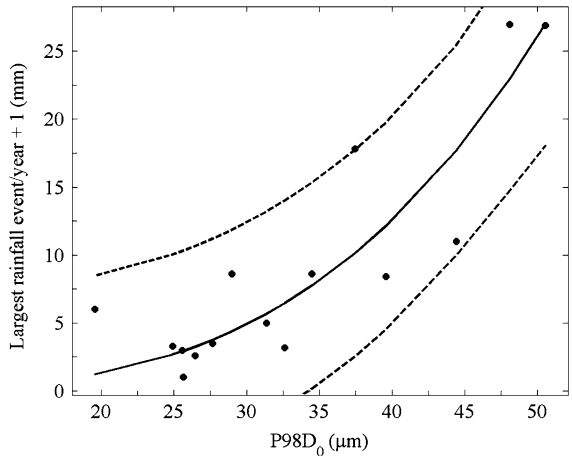

Fig. 6 Linear regression between log-transformed $P98D_0$ and largest rainfall event/year at Rea Point (1985–1971) using robust estimation, and the 90 % confidence interval (*dotted lines*)

The correlations with other PSD indices are weaker than those obtained for $P98D_0$, except for sD_0, which is itself strongly correlated with $P98D_0$.

Climate reconstruction

We use the log–log model (Eq. 2) to reconstruct rainfall amount for the last 2845 years. However, we present the reconstruction for only the period after ~AD 244, when the coring site was fully lacustrine, to avoid complications related to possible changes in sedimentological and geomorphological conditions (Fig. 7). The reconstructed rainfall amount was quite steady from AD 244 until 1900 (Fig. 7), whereas the twentieth century appears as a strong positive anomaly. In detail, precipitation during the period between AD 400 and 1050 was generally below average, except for the sixth and the seventh centuries. Another period

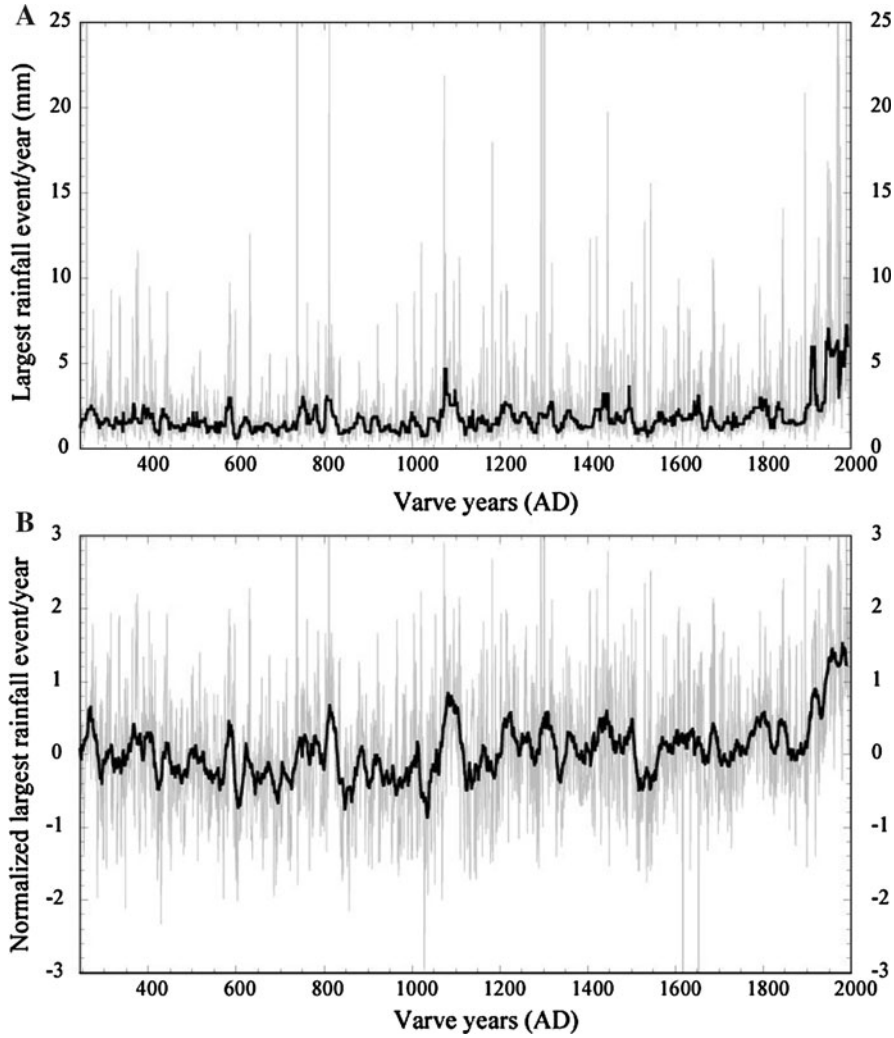

Fig. 7 **A** Reconstructed largest annual rainfall amounts (mm) for the past 1,750 years using the log–log transformed. The *grey line* is the raw data and the *black line* is the 15-years running median filter. **B** Reconstructed largest annual rainfall anomalies using the log–log transformation. The *grey line* is the raw data and the *black line* is the 15-years running mean

of high precipitation was centered around AD 1100. After AD 1200, precipitation amount was generally above or near average, with the exception of AD 1500–1550. The precipitation amounts were average during the second half of the nineteenth century, but increase substantially for the rest of the record.

Discussion

Chronology

Comparison between our chronology and the original from Cuven et al. (2011) shows an overall difference of 2.6 % (72 years) for the upper 360 cm (Fig. 3). Discrepancies are more pronounced over intervals with very thin laminae (0.3 mm). These fine varves are difficult to delineate using thin-sections images compared with SEM images, which have better phase contrast and higher resolution. In these intervals, the counts based on SEM images were systematically and logically higher. We conclude that the new chronology is an improvement over the previous one. These results also highlight the value for SEM imagery for thin, fine-grained varves.

Cuven et al. (2011) identified eight likely erosive beds in the remainder of the 423-cm-long laminated sequence, and these have also been recognized in our BSE images. All of these units are thinner and finer-grained than the uppermost bed that is believed to have eroded 5 years of sediment, and they lack erosional features at the microscopic scale. We thus infer that our varve chronology is minimally affected by high-energy sedimentary events.

Climatic interpretation of the grain-size record at Cape Bounty

The significant and strong correlation between $P98D_0$ at East Lake and rainfall events at Rea Point is consistent with process studies at Cape Bounty, a study area with the longest record of process-oriented observations in the Arctic. For instance, Dugan et al. (2009) demonstrated the important impact of two rainfall events (9.2 and 10.8 mm) that occurred in late June and July 2007 on the West River. They showed that these rain events generated peak discharge and suspended sediment transport two times larger than the nival melt in the same year. They also reported that downstream sediment traps recorded the rainfall as a hyperpycnal-flow deposit with the highest sediment deposition rate of the season and the coarsest mean grain size. Their results also demonstrated the importance of prior moisture conditions and the role of permafrost active-layer development as an important factor controlling rainfall runoff and sediment transport response to precipitation events.

Our observations and climate correlations with varve properties are in agreement with these monitoring results (Dugan et al. 2009; Lewis et al. 2011). The largest rainfall events at Rea Point were recorded late in the summer season in AD 1971 (25.9 mm) and 1973 (when 13 mm fell twice within 2 days) (Fig. 8). In those years, warm conditions prevailed before the precipitation events (Fig. 8). For instance, maximum temperatures reached uncommon values (>13 °C) during the 4 days before the major rainfall event that occurred on July 30, 1971 (Fig. 8). Similarly, warm conditions were recorded in early August AD 1973 before the high rainfall events (Fig. 8). During the calibration period, the highest $P98D_0$ was measured in varves deposited during these two wet and warm years (Fig. 9). Our record is also sensitive to summer rain events in more typical years, such as AD 1978. This was an average year in terms of MDD; it experienced an average rainfall event (7.6 mm) on 215 JD (Fig. 8) that was sufficient to produce a sedimentary response, i.e. a small debris flow (Fig. 9).

Cape Bounty seems to be one of the few reported Arctic varved sequences to be sensitive to rainfall events. However, the overall paucity of long-term monitoring of river discharge and sediment yield in lakes, and the general focus on nival runoff and summer glacial melt may have led to a biased view of processes within lake catchments in the High Arctic. These precipitation events clearly trigger substantial suspended sediment yields in High Arctic lakes (Church 1972, 1974, 1988; Cogley and McCann 1976; Lewkowicz and Wolfe 1994; Lewis et al. 2005, 2011; Dugan et al. 2009). In sum, we argue that the primary climate signal stored in Cape Bounty sediments are large summer rain events and are recorded by high $P98D_0$, particularly when warm conditions predate the rain events.

The autocorrelation of VT and the PSD indices likely indicates some hysteresis in the sediment yield at Cape Bounty, as was described at Nicolay Lake, a similar Arctic watershed (Lamoureux 2002). While it does not change the strength of the correlations established in this study (Table 2), this geomorphic signal should be considered carefully in similar studies.

High-energy facies characterization using image analysis

High-energy deposition events (turbidites and debris flow) identified by Cuven et al. (2010) can be distinguished by their coarse $P98D_0$ and sD_0 (Fig. 10). The bases of turbidites have been similarly characterized by high $P99D_0$ and sD_0 values in the

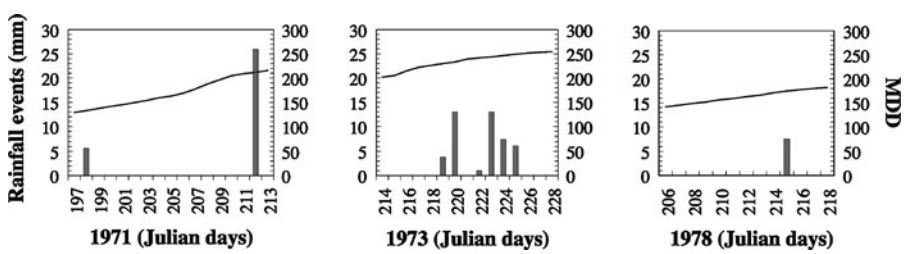

Fig. 8 Examples of 3 years (1971, 1973, and 1978) with extreme daily rainfall events (*vertical bars*) at Rea Point, Nunavut, with cumulative MDD (*curved line*). Data are from the National Climatological Archive (NCA) of Meteorological Service Canada (MSC)

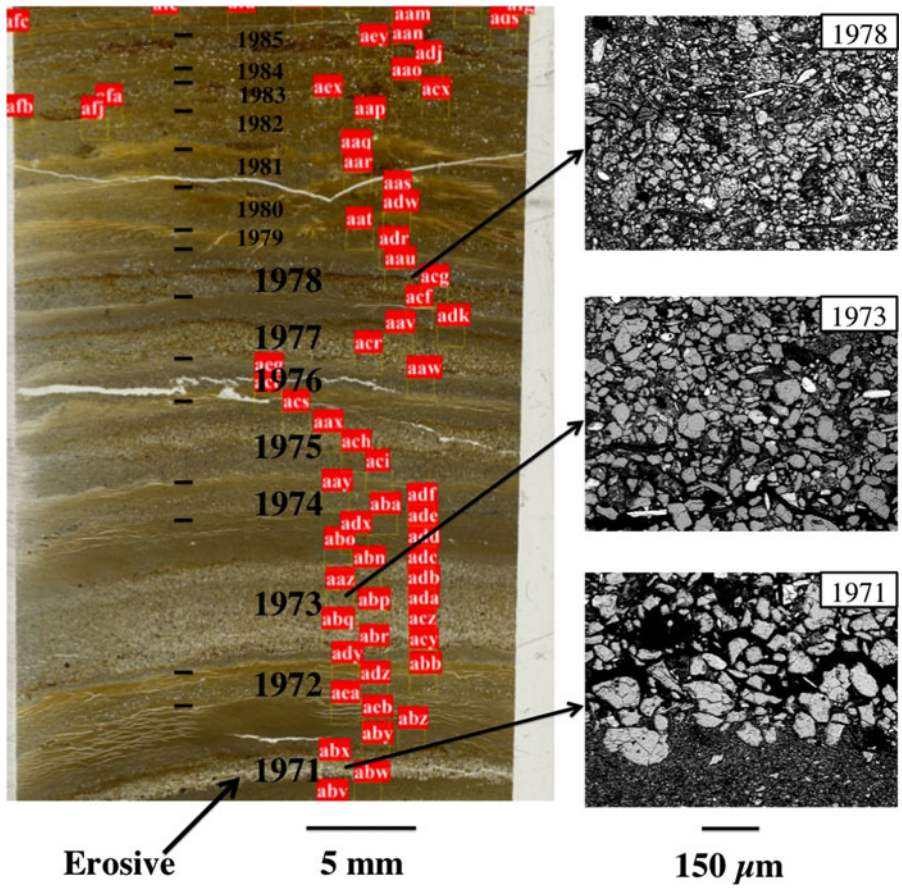

Fig. 9 Sedimentary structures corresponding to years AD 1971–1985, a period that encompasses major turbidites and debris flow. Thin-section image (*left*) with regions of interest (ROIs; *yellow squares*) and varve boundaries (*horizontal black lines*). The *right panel* shows backscatter electron images of sediment deposited during years AD 1971, 1973, and 1978 (ROIs abx, aaz, and aau respectively) that contain thick laminae with coarse grain size. Other years (AD 1975, 1977, and 1985) with rainfall signals also exhibit coarse grain size. The base of the turbidite formed in AD 1971 shows an erosive lower contact. (Color figure online)

sedimentary sequence from South Sawtooth Lake, Ellesmere Island (Lewis et al. 2010). The base of a turbidite is typically poorly sorted and coarse grained in the head and the body of the energetic turbiditic flow, whereas finer sediment is deposited afterwards, as the flow wanes and deposition occurs through particle settling (Reading 1996). Lewis et al. (2010) interpreted this facies as deposited by hyperpycnal flow and likely generated by rainfall events. The coarse sD_0 and $P98D_0$ values observed here appear to reflect this unsorted coarse sediment at the base of turbidite facies. On the other hand, debris flows are primarily composed of viscous mixtures of sediment and water in which the volume and mass of sediment exceeds that of water (Major 2003). Because the absence of turbulence generates no dynamic sorting of material, the resulting deposit is poorly sorted (Nichols 2009). The sharp increase of both $P98D_0$ and sD_0 during the twentieth century (Fig. 4) is in agreement with observations from thin-sections in which turbidites and debris-flow deposits can be identified (Fig. 9). In sum, high values of $P98D_0$ and sD_0 are observed within both turbidites and debris-flow deposits (Fig. 10).

Particle-size versus varve-thickness variations

PSD and VT are significantly correlated, but the strength of correlations is weak (Table 1). The weak correlation was previously noted by Francus et al. (2002) who hypothesized that the decoupling of VT and grain size reflects the fact that VT is the sum of many different phenomena occurring throughout the year, whereas grain size can be related to single events, and hence better linked with the instrumental record. This was confirmed by the recent process study by Cockburn and Lamoureux (2008a) at Cape Bounty showing that the size of the coarser fraction collected in sediment traps tracks the high-energy flows better than the short-term mass accumulation.

The long-term evolution of VT and PSD indices at Cape Bounty is strikingly different (Fig. 4). At Cape

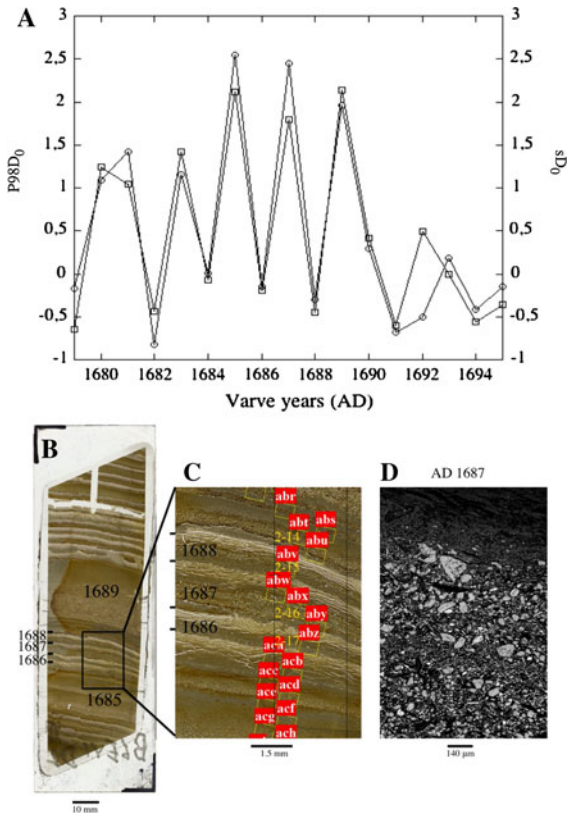

Fig. 10 **A** Time series (AD 1695–1679) of normalized $P98D_0$ (*open circle*) and sD_0 (*open square*). **B** Thin-section of sediment deposited during the interval in **A**, showing two prominent turbidites at AD 1689 and 1685. **C** Blow-up of three thin varves from AD 1688 to 1686. Varves formed during AD 1688 and 1686 have low $P98D_0$ and sD_0 values, whereas AD 1687 has high values. **D** Backscatter electron image of varve formed in AD 1687, showing coarse grain size interpreted as a debris-flow deposit

Bounty, several working hypotheses can be suggested to explain this decoupling. The geomorphic evolution of the lake and its watershed is controlled by the slow and progressive glacioisostatic rebound as inferred from geochemical and sedimentological properties of the 7.4-m-long core (Cuven et al. 2011). The increase in varve thickness between AD 200 and 500 cannot be due to a change in the tributary competence because there is no simultaneous change in our PSD indices. The clear step change in mD_0 around AD 1350 does not correspond to a detected change in known boundary conditions in the watershed. This change could be climatically driven, although no particular trend in climate has been documented around this time in the region. Alternatively, the coarser sediment could result from progradation of the East Lake inflow delta during this period, which in turn would effectively increase the proximity of the core site, the sedimentation rate and the coarseness of the sediment (Cuven et al. 2011). However, such a change is expected to be progressive, which is not the case. An alternate mechanism entails the progressive flushing of the salt water from what is assumed to have been a meromictic lake, which could have switched sediment delivery from overflows to underflows, and resulted in the deposition of coarser sediment in the core locations.

Discussion of correlation with climate instrumental record

Rea Point is the closest weather station to Cape Bounty (100 km east). Despite its short duration, it offers one of the strongest, if not the strongest, correlation between an instrumental record and varve properties yet discovered in the Arctic. Our study is the first to demonstrate a correlation between rainfall events and clastic varves in this region. This linkage is not surprising because rainfall events are important quasi-annual events recorded in most Arctic varves records (Lamoureux 2000; Lewis et al. 2005). Soils in these cold regions support sparse vegetation and are frozen at depth, which limits water infiltration and can create a substantial runoff response when precipitation occurs (Church 1988; Lamoureux 2000). Furthermore, the western part of the Canadian High Arctic was more affected by the overall increase of precipitation during the second half of the twentieth century as observed by the coupled model intercomparison project phase 3 (CMIP3) (Min et al. 2008).

Because the Rea Point record is short (1969–1985), we investigated the possibility of using the longer record from Mould Bay instead. The largest rainfall events at Mould Bay and Rea Point are not correlated ($r = -0.04$, $\rho = 0.01$, $\tau = -0.03$, $p > 0.9$ for all coefficients) (not shown in Table 2), while annual rainfall shows a weak and insignificant relationship ($r = 0.41$, $\rho = 0.17$, $\tau = 0.15$, with $p = 0.13, 0.55, 0.46$, respectively). On the other hand, June temperatures and MDD significantly correlate (June temperatures: $r = 0.87$, $\rho = 0.65$, $\tau = 0.46$ and MDD: $r = 0.70$, $\rho = 0.70$, $\tau = 0.47$, with maximal $p < 0.02$) between Rea Point and Mould Bay. Similarly, mean air temperature at Cape Bounty is strongly correlated with Mould Bay for the monitoring period (2003–2009) ($r^2 = 0.92$; SE = 3.5) (Lewis et al. 2011). Collectively, these observations suggest a

common regional pattern for temperatures that can be used for correlation with sedimentary data. Additionally, $P98D_0$ positively and significantly correlates with June temperatures at Mould Bay (Table 2), although these correlations are weaker than for precipitation.

None of the sedimentary properties seems to be directly linked to snow accumulation instrumental record (Table 2). At Cape Bounty Lewis et al. (2011) noted that the East Lake catchment has fewer concave surfaces favorable to accumulate snow (Fig. 1). This geomorphological property implies that redistribution of snow by winds is important, and may impede a quantitative link between snow water equivalent and sediment transport.

In sum, sediment properties at Cape Bounty can mainly be explained by rain events in summer, with some influence of temperature and snow melt.

Climatic reconstruction

Few Arctic reconstructions of rainfall have been published to compare with our record. Of note is the amount of summer rainfall at Cape Bounty during the twentieth century, which is unprecedented in the last 1750 years. As such, the precipitation of the twentieth century in the western Arctic Archipelago is anomalous, analogous to summer temperature over the entire Arctic (Kaufman et al. 2009). Likewise, the sharp peak centered around AD 1100 (Fig. 7) appears to be consistent with the increase of temperature that occurred around AD 1000 and 1100 according to the temperature reconstruction from Moberg et al. (2005). The similarity between our precipitation record and the temperature record is not surprising because higher temperature allows for more moisture to be stored in the atmosphere. Moreover, warmer temperature may favor the decline of sea-ice cover over the nearby Arctic Ocean, allowing for more evaporation. Finally, as described above, warmer temperatures also have a positive feedback on the sensitivity of East Lake to summer precipitation by increasing the depth of the active layer (Lewis et al. 2011). Other prominent features of our record are linked with difficulty to climate forcings and other records.

Image analysis

This work highlights the potential of using annually resolved PSD to reconstruct past precipitation amounts. These parameters have been rarely investigated because of technical challenges that limited the generation of long time series from SEM image sets. The advantage of using this imaging technique is that very thin laminae, down to 0.3 mm, can be accurately measured. This type of measurement is not influenced by sediment compression with increasing depth, and individual laminations can be measured without the contamination from neighboring laminae, which is often the case with traditional subsampling techniques (Lotter et al. 1997). This procedure is applicable to long records that take advantage of new software with substantial analytical efficiencies. In the case of East Lake, PSD indices are more strongly correlated with climate parameters than is VT. Revisiting key sites from the Arctic using this innovative technique may increase fidelity of long-term proxy climate records.

Conclusion

Annually resolved PSD obtained using image analysis provided a 1750-year-long quantitative reconstruction of summer rain events from East Lake in the Canadian High Arctic. Correlations of $P98D_0$ with the instrumental record yielded one of the strongest correlations obtained to date in the Arctic ($r = 0.85$), which is also higher than varve thickness from the same site. Rain events in the western Canadian Arctic Archipelago increased to unprecedented levels in the twentieth century compared to the last 1750 years.

Acknowledgments This work was supported by the Canadian Federal program for the international polar year (IPY) and by research grant of NSERC to Pierre Francus and Scott Lamoureux. Logistical support was provided by the Polar Continental Shelf Project, Natural Resources Canada (PCSP). Special thanks to David Fortin and Anna Pienkowski-Furze for core processing. Thanks to Arnaud De Coninck for help with the SEM and Laurence Provencher-Nolet for image analysis. The authors are grateful for the suggestions of Antti Ojala, the editorial comments of Darrell Kaufman and helpful input of two anonymous reviewers.

References

Abdi H (2007) The Kendall rank correlation coefficient. In: Salkind NJ (ed) Encyclopedia of measurement and statistics. Sage, Thousand Oaks, pp 508–510

Box GEP, Cox DR (1964) An analysis of transformations. J R Stat Soc 26:211–252

Church M (1972) Baffin Island sandurs: a study of Arctic fluvial processes. Geological Survey of Canada, Department of Energy, Mines and Resources, Ottawa

Church M (1974) Hydrology and permafrost with reference to North America. In: Workshop seminar on permafrost hydrology, Environment Canada, pp 7–20

Church M (1988) Floods in cold climates. In: Baker VR, Kochel CR, Patton PC (eds) Flood geomorphology. Wiley, New York, p 528

Cockburn J, Lamoureux S (2008a) Inflow and lake controls on short-term mass accumulation and sedimentary particle size in a High Arctic lake: implications for interpreting varved lacustrine sedimentary records. J Paleolimnol 40(3):923–942

Cockburn JMH, Lamoureux SF (2008b) Hydroclimate controls over seasonal sediment yield in two adjacent High Arctic watersheds. Hydrol Process 22(12):2013–2027

Cogley JG, McCann S (1976) An exceptional storm and its effects in the Canadian High Arctic. Arct Alp Res 8:105–110

Cook RD, Weisberg S (1982) Residuals and influence in regression. Springer, New York, p 240

Cuven S, Francus P, Lamoureux SF (2010) Estimation of grain size variability with micro X-ray fluorescence in laminated lacustrine sediments, Cape Bounty, Canadian High Arctic. J Paleolimnol 44(3):803–817

Cuven S, Francus P, Lamoureux S (2011) Mid to Late Holocene hydroclimatic and geochemical records from the varved sediments of East Lake, Cape Bounty, Canadian High Arctic. Quat Sci Rev 30(19–20):2651–2665

De Keyser TL (1999) Digital scanning of thin sections and peels. J Sediment Res 69(4):962–964

Dugan HA, Lamoureux SF, Lafrenière MJ, Lewis T (2009) Hydrological and sediment yield response to summer rainfall in a small high Arctic watershed. Hydrol Process 23(10):1514–1526

Folk RL, Ward WC (1957) Brazos River bar: a study in the significance of grain size parameters. J Sediment Petrol 27(1):3–26

Francus P (1998) An image-analysis technique to measure grain-size variation in thin sections of soft clastic sediments. Sediment Geol 121(3–4):289–298

Francus P, Karabanov E (2000) A computer-assisted thin-section study of Lake Baikal sediments: a tool for understanding sedimentary processes and deciphering their climatic signal. Int J Earth Sci 89(2):260–267

Francus P, Nobert P (2007) An integrated computer system to acquire, process, measure and store images of laminated sediments. In: 4th International limnogeology congress, Barcelona, 11–14th July

Francus P, Prirard E (2004) Testing for sources of errors in quantitative image analysis. In: Francus P (ed) Image analysis, sediments and paleoenvironments. Kluwer Academic Publisher, Dordrecht, The Netherlands, pp 87–102

Francus P, Bradley RS, Abbott MB, Patridge W, Keimig F (2002) Paleoclimate studies of minerogenic sediments using annually resolved textural parameters. Geophys Res Lett 29(20):1998

Francus P, Bradley R, Lewis T, Abbott M, Retelle M, Stoner J (2008) Limnological and sedimentary processes at Sawtooth Lake, Canadian High Arctic, and their influence on varve formation. J Paleolimnol 40(3):963–985

Hodgson D (1989) Quaternary geology of the Queen Elizabeth Islands. In: Fulton RJ (ed) Quaternary geology of Canada and Greenland, vol 1. Geological Survey of Canada, Geology of Canada, pp 441–478

Hodgson D, Vincent JS, Fyles JG (1984) Quaternary geology of central Melville Island, northwest territories. Geological Survey of Canada Paper 83-16, Geology of Canada, p 23

Kaufman DS, Schneider DP, McKay NP, Ammann CM, Bradley RS, Briffa KR, Miller GH, Otto-Bliesner BL, Overpeck JT, Vinther BM (2009) Recent warming reverses long-term Arctic cooling. Science 325:1236–1239

Kaufman CA, Lamoureux SF, Kaufman DS (2011) Long-term river discharge and multidecadal climate variability inferred from varved sediments, southwest Alaska. Quat Res 76(1):1–9

Lamoureux S (2000) Five centuries of interannual sediment yield and rainfall-induced erosion in the Canadian High Arctic recorded in lacustrine varves. Water Resour Res 36(1):309–318

Lamoureux S (2002) Temporal patterns of suspended sediment yield following moderate to extreme hydrological events recorded in varved lacustrine sediments. Earth Surf Process Land 27:1107–1124

Lamoureux SF, McDonald DM, Cockburn JMH, Lafrenière MJ, Atkinson DM, Treitz P (2006) An incidence of multi-year sediment storage on channel snowpack in the Canadian High Arctic. Arctic 59:381–390

Laurin E (2010) The impact of experimental snow augmentation on soil thermal regimes and nutrient fluxes from High Arctic headwater catchments. Unpublished MSc. thesis, Queen's University, Kingston, p 148

Lewis T, Braun C, Hardy DR, Francus P, Bradley RS (2005) An extreme sediment transfer event in a Canadian High Arctic stream. Arct Antarct Alp Res 37(4):477–482

Lewis T, Francus P, Bradley RS, Kanamaru K (2010) An automated system for the statistical analysis of sediment texture and structure at the micro scale. Comput Geosci 36:1374–1383

Lewis T, Lafrenière MJ, Lamoureux SF (2011) Hydrochemical and sedimentary responses of paired High Arctic watersheds to unusual climate and permafrost disturbance, Cape Bounty, Melville Island, Canada. Hydrol Process. doi: 10.1002/hyp.8335

Lewkowicz AG, Wolfe PM (1994) Sediment transport in hot weather creek, Ellesmere Island, NWT, Canada, 1990–1991. Arct Alp Res 26:213–226

Lotter A, Sturm M, Teranes J, Wehrli B (1997) Varve formation since 1885 and high-resolution varve analyses in hypertrophic Baldeggersee (Switzerland). Aquat Sci Res Across Bound 59(4):304–325

Major JJ (2003) Debris flow. In: Middleton GV (ed) Encyclopedia of sediments and sedimentary rocks. Kluwer, Dordrecht, pp 186–188

Maronna RA, Martin RD, Yohai VJ (2006) Robust statistics. Wiley, Chichester

McDonald DM, Lamoureux SF (2009) Hydroclimatic and channel snowpack controls over suspended sediment and grain size transport in a High Arctic catchment. Earth Surf Process Land 34(3):424–436

Min SK, Zhang X, Zwiers F (2008) Human-induced Arctic moistening. Science 320:518–520

Moberg A, Sonechkin DM, Holmgren K, Datsenko NM, Karlén W (2005) Highly variable Northern Hemisphere temperatures reconstructed from low-and high-resolution proxy data. Nature 433(7026):613–617

Moritz RE, Bitz CM, Steig EJ (2002) Dynamics of recent climate change in the Arctic. Science 297:1497–1502

Nederbragt A, Thurow J (2004) Digital sediment colour analysis as a method to obtain high resolution climate proxy records. In: Francus P (ed) Image analysis, sediments and paleoenvironments. Kluwer Academic Publisher, Dordrecht, The Netherlands, pp 105–124

Nichols G (2009) Sedimentology and stratigraphy. Wiley-Blackwell, Chichester

Overpeck J, Hughen K, Hardy D, Bradley R, Case R, Douglas M, Finney B, Gajewski K, Jacoby G, Jennings A (1997) Arctic environmental change of the last four centuries. Science 278:1251–1256

Pautler BG, Simpson AJ, Mcnally DJ, Lamoureux SF, Simpson MJ (2010) Arctic permafrost active layer detachments stimulate microbial activity and degradation of soil organic matter. Environ Sci Technol 44(11):4076–4082

Reading HG (1996) Sedimentary environments: processes, facies and stratigraphy. Wiley-Blackwell, Malden

Rousseeuw PJ, Leroy AM (1987) Robust regression and outlier detection. Wiley Online Library, New York

Sheather SJ (2009) A modern approach to regression with R. Springer, New York

Shumway RH, Stoffer DS (2000) Time series analysis and its applications. Springer, New York

Soreghan MJ, Francus P (2004) Processing backscattered electron digital images of thin section. In: Francus P (ed) Image analysis, sediments and paleoenvironments. Kluwer Academic Publisher, Dordrecht, The Netherlands, pp 203–225

Stewart KA, Lamoureux SF (2011) Connections between river runoff and limnological conditions in adjacent high Arctic Lakes: Cape Bounty, Melville Island, Nunavut. Arctic 64(2):169–182